Onset of perpendicular magnetization in nanostripe arrays of Fe on stepped W(110) surfaces

H. J. Elmers
Johannes Gutenberg-Universität Mainz, Staudingerweg 7, D-55099 Mainz, Germany

J. Hauschild and U. Gradmann
Technische Universität Clausthal, Leibnizstrasse 4, D-38678 Clausthal-Zellerfeld, Germany
(Received 18 June 1998)

Nanostripe arrays of alternating double layer and monolayer stripes of Fe(110) films were grown on stepped W(110) surfaces. The magnetic easy axis in the as-prepared samples switches from in-plane in the monolayer to perpendicular in the double layer stripes. Beyond a critical width, which is determined by exchange interactions, the double layer stripes show remanent perpendicular order. Magnetostatic interactions induce antiferromagnetic interstripe coupling, which suppresses perpendicular remanence at higher coverages. During residual gas exposure, the double layer easy axis is rotated into the plane, resulting in a sharp transition from antiferromagnetic to ferromagnetic interstripe coupling. [S0163-1829(99)01705-1]

I. INTRODUCTION

The possibility to tailor perpendicular composition profiles of epitaxial magnetic films, i.e., multilayers, provides an enormous impact on the progress of the understanding of magnetism. The discovery of exchange coupling through a nonmagnetic spacer[1–3] and giant magnetoresistance[4,5] is based on these techniques to prepare perpendicular profiles of both composition and magnetic properties on a nanoscale. Recently, the concepts of perpendicular nanostructures have been extended to lateral magnetic nanostructures, i.e., two-dimensional arrays of magnetic nanowires or nanostripes, which can be prepared either by lithography[6,7] or by self-organized growth on grooved[8] or on vicinal single crystal substrates.[9–11] Nanostripes of Fe atoms grown on vicinal W(110) substrates have revealed a new type of superferromagnetic phase transition.[11]

In the present article, we focus on pseudomorphic Fe(110) nanostripes grown on vicinal W(110) substrates in the thickness range between 1 and 2 atomic layers (AL). When grown at room temperature on smooth W(110) substrates, these *sesquilayers* consist of a nearly perfect monolayer with islands of the second layer on top. For these structures a frustration of remanent in-plane order was found,[12] originally interpreted as a spin-glass-like phase. However, in-plane remanence with outstanding strong coercivities was observed in similar samples by other groups,[13–15] in combination with unconventional time-dependence of the magnetic reversal,[14] and unusual elastic properties.[15] Accordingly, an interpretation of the frustration phenomena described in Ref. 12 in terms of magnetic freezing was proposed.[13,15] A kinetic Ising model on structures similar to the experimentally observed ones explains these findings without the assumption of unusual anisotropies.[16] Recently, torsion oscillation magnetometry[17,18] revealed a perpendicular anisotropy in the double layer islands, in sharp contrast to the easy-plane anisotropy in the monolayer. The perpendicular anisotropy was explained as a magnetoelastic contribution resulting from the huge epitaxial strain (10%) in the pseudomorphic Fe film.[17] The interplay between double layer islands and monolayer regions with orthogonal anisotropies, interconnected on a nanometer scale, gives a qualitative explanation for the unusual magnetic properties, but makes the Fe sesquilayer system extremely complicated in detail. Moreover, a rapid degradation of the perpendicular anisotropy with increasing residual gas exposure has been observed.[19] A spectroscopic scanning tunneling microscopy (STM) study[20] reveals a sudden change of the electronic structure in the double layer (DL) islands with increasing exposure.

Basically the same phenomena of perpendicular magnetization in pseudomorphic double layers and in-plane uniaxial anisotropy in monolayers has been observed in periodic nanostripe arrays grown on vicinal W(110) substrates.[21] The reduced dimension opens an easy approach to a micromagnetic interpretation of the observed phenomena.[22]

The aim of this article is to provide a detailed understanding of the magnetic sesquilayer phenomena for the one-dimensional case of periodic stripe structures. The article is organized as follows. In the next section we describe the experimental setup. Section III describes how to prepare the samples. Section IV reports the experimental results. A discussion of the magnetic properties as a function of temperature and coverage is given in Sec. V A. The change of magnetic properties during adsorption of residual gas is discussed in Sec. V B.

II. EXPERIMENT

Experiments were done in a UHV system providing two sample stages with a base pressure of 1×10^{-10} Torr. At sample stage A samples could be prepared using molecular beam epitaxy at pressures $p_p<5\times10^{-10}$ Torr and characterized structurally and chemically using low-energy electron diffraction (LEED) and Auger spectroscopy (AES). Magnetic measurements were done at the same stage by means of Kerr magnetometry (MOKE). Using two separate lasers, we measured both the ellipticity ϵ_K of the longitudinal Kerr effect in longitudinal fields applied along the $[1\bar{1}0]$ direction (magnetic easy axis of the monolayer), and the rotation θ_K of the polar effect in polar fields. Using a compensation

technique,[23] both ϵ_K and θ_K were measured in absolute units. At stage A the substrate crystal could be heated up to 2000 K by electron bombardement, and cooled down to 130 K using liquid nitrogen. Temperatures were measured with a relative accuracy of 1 K and an absolute accuracy of about 10 K using a thermocouple fitted to the sample holder. The temperature could be stabilized at 165 ± 10 K for extended periods. MOKE measurements presented in this study were carried out either at this stabilized temperature or during slowly warming up at a rate of about 1 K/min. At the second sample stage (stage B) samples could be characterized by scanning tunneling microscopy (STM) at room temperature. Samples could be transferred *in situ* between those two stages.

III. PREPARATION AND CHARACTERIZATION OF SAMPLES

The vicinal W(110) substrates were polished *ex situ* and cleaned *in situ* by heating to 2000 K. Carbon segregations were oxidized by heating to 1200 K in an oxygen atmosphere of 10^{-8} Torr prior to the preparation of a series of samples. The clean crystal surface shows monoatomic steps only, with some dispersion of the terrace width of the order of 30%. All samples presented in this study were deposited on vicinal W(110) substrates, with atomic steps along [001] and a mean step distance of $w_0 = 9$ nm, corresponding to $W_0 = w_0\sqrt{2}/a_W = 40$ AR (atomic rows) with lattice constant $a_W = 0.316$ nm. The value of W_0 was chosen because we wanted to avoid misfit dislocations, which were observed[12,25] in elongated double layer islands with a width greater than 9 nm.

Fe was deposited at 700 K with a growth rate of $R = 0.3$ AL/min. A 10 MHz quartz balance monitored the relative Fe coverage. The calibration of the absolute coverage was performed via STM with an accuracy of 5%. Characterizing the cleanliness of the preparation by a quality factor which we define as $Q = R/p_p =$ thickness/exposure, we prepared the films with Q better than 10 AL/Langmuir (1 Langmuir $= 10^{-6}$ Torr sec).

The morphology of the films was checked by STM. Figure 1 shows a sample with coverage $\Theta = 1.8$ AL. With the growth parameters described above, the Fe grows in step flow from the W steps until 2 AL are complete, forming arrays of smooth pseudomorphic stripes of alternating monolayer (ML) and double layer (DL) height, without any indication of misfit dislocations. The STM image shown in Fig. 1 was taken after an exposure of more than 3 Langmuirs of residual gas. In DL areas we observed a regular (110) lattice feature [see Fig. 1(b)] with a lattice constant twice that of the tungsten lattice constant a_W, corresponding to a 2×2 superstructure. Presumably, this regular structure, which is disturbed by only a few dark irregularities, is induced by adsorption of CO molecules. In ML areas the 2×2 superstructure is of significantly reduced regularity. This decoration effect is the main source of the contrast between ML and DL areas observed in Fig. 1.

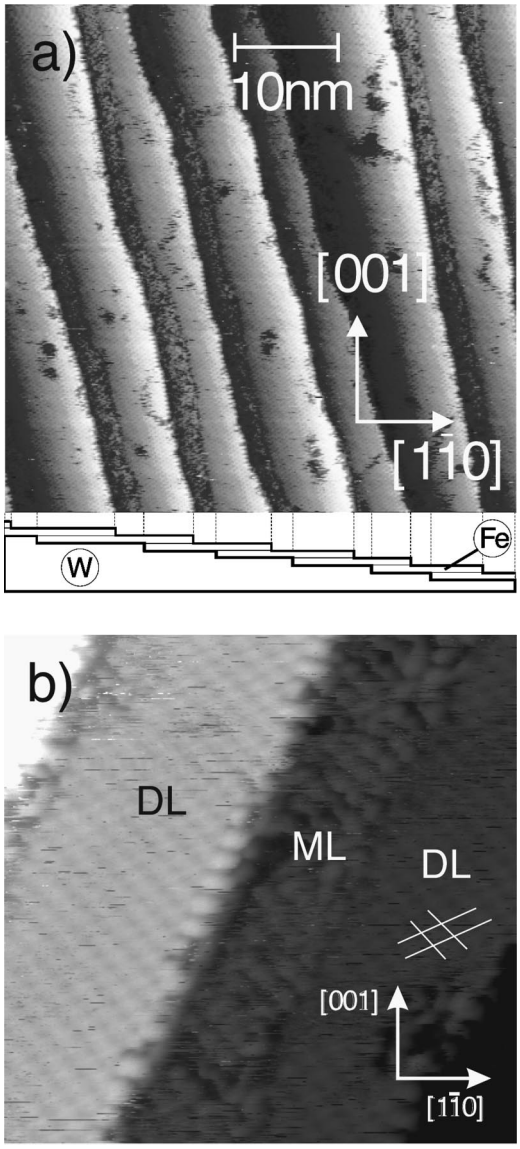

FIG. 1. (a) STM image of a sample of coverage $\Theta = 1.8$ atomic layers. A schematic cross section of the sample cut at the bottom line is shown below the image. The dotted lines indicate the borderlines between double layer (DL) and monolayer (ML) stripes. (b) Zoomed region (10 nm$\times$10 nm) of (a). Thin lines indicate the $\langle 111 \rangle$ directions of the 2×2 superstructure. The shearing in (a) and (b) caused by a drift of the STM scanner was not corrected. Whereas the $[1\bar{1}0]$ axis is not changed the actual [001] axis lies paralled to the borderlines between ML and DL regions in both (a) and (b).

IV. MAGNETIC RESULTS

For a measurement of the onset of perpendicular magnetization we prepared wedge-shaped samples with linearly increasing Fe thickness from $\Theta = 0.9$ AL to $\Theta = 1.4$ AL and a baseline length of 3 mm. Immediately after preparation the samples were cooled down to the stabilized temperature of (165 ± 10) K. Polar Kerr loops were then measured at (165 ± 10) K. The external field was limited to 200 mT. The insets in Figs. 2(a) and 2(b) show typical loops. To characterize the loops we defined parameters as indicated in the insets. We used remanent values $\theta_{K,r}$, extrapolated values $\theta_{K,e}$, resulting from extrapolation of the high field linear sections to the vertical axis, and the susceptibility $\chi_f = d\theta_{K,r}/d(\mu_0 H)|_{\text{high field}}$ measured for the highest fields of those linear sections. These parameters are shown in Figs.

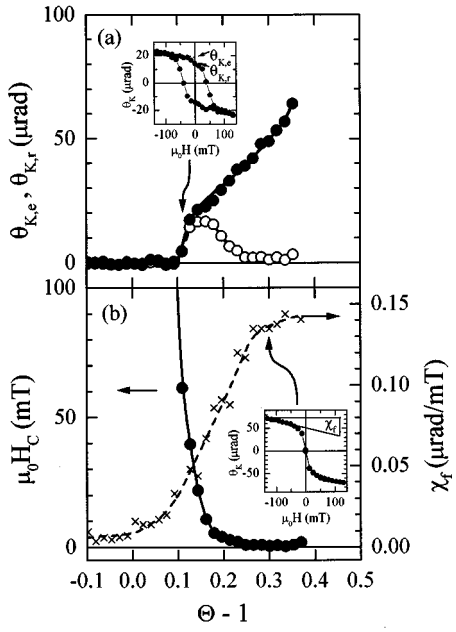

FIG. 2. (a) Remanent and extrapolated Kerr rotation $\theta_{K,r}$ (open circles) and $\theta_{K,e}$ (full circles) as a function of double layer coverage $\Theta-1$, measured at a temperature $T=165$ K. The inset shows a single Kerr loop of the series indicates how $\theta_{K,r}$ and $\theta_{K,e}$ were determined from the polar Kerr loops. (b) Coercive force H_c (full circles) and final susceptibility $\chi_f=\partial\theta_K/\partial\mu_0 H$ (crosses) at the maximum available field $\mu_0 H_{max}=120$ mT (as indicated in the inset) versus double layer coverage $\Theta-1$.

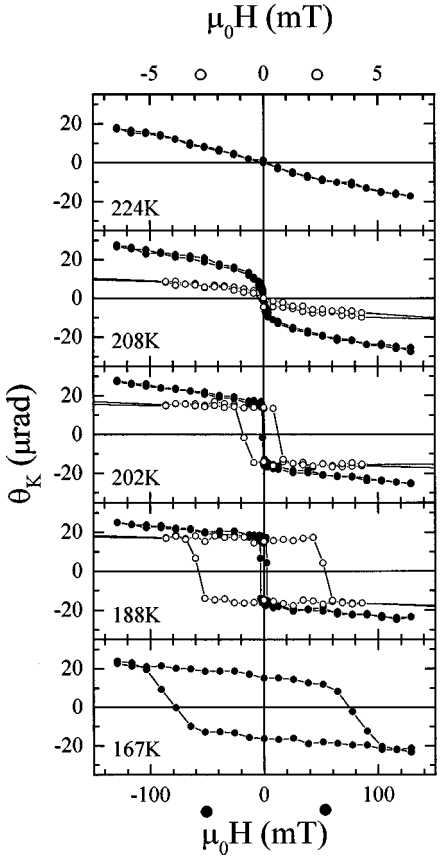

FIG. 3. Polar Kerr loops for a sample of coverage $\Theta=1.2$ measured at temperatures T as indicated in the figure. Full symbols correspond to the data plotted on the full field scale at the bottom, open symbols correspond to the same data plotted on an expanded field scale at the top of the figure.

2(a) and 2(b), respectively, as a function of the double layer coverage $\Theta-1$. Using the mean step distance $W_0=40$ AR, a coverage of $\Theta=1.1$ AL corresponds to a mean DL stripe width of $W_{\mathrm{DL}}=W_0(\Theta-1)=4$ AR. Below $\Theta=1$ the polar Kerr signal is nearly zero with a small residual linear increase χ_f with external field. The nearly constant value of $\chi_f(ML)=0.005$ μrad/mT for $\Theta<1$ can be explained as the initial section of a hard axis loop for the complete Fe monolayer with an in-plane easy axis. Our available field is much smaller than the saturation field H_a, which can be calculated from $\chi_f(ML)$ assuming a saturation value $\theta_{K,s}=100$ μrad/AL, as estimated from $\theta_{K,e}$ for Θ approaching the complete double layer. We then obtain the result $\mu_0 H_a=\theta_{K,s}/\chi_f(ML)=20$ T as a measure for the out-of-plane anisotropy field of the monolayer, in rough agreement with values reported previously.[12] Above $\Theta=1$, χ_f shows a nonlinear increase. Both remanence $\theta_{K,r}$ and extrapolation $\theta_{K,e}$ disappear for $\Theta<1.1$, and discontinuously jump at $\Theta=1.1$ to a nearly common value of 18 μrad, which indicates approximate squareness of the loop, as shown in the inset of Fig. 2(a). In coincidence with the onset of $\theta_{K,e}$, the coercive force H_c diverges upon approaching $\Theta=1.1$ from higher coverages. At higher coverages $\Theta>1.1$ the extrapolation $\theta_{K,e}$ increases linearly, whereas both the remanence $\theta_{K,r}$ and H_c decrease towards zero.

In order to measure the temperature dependence of the magnetic behavior we prepared single films of homogeneous thickness. The samples were cooled down to $T=135$ K immediately after preparation and polar Kerr loops were taken during warming up. Loops for an example with $\Theta=1.2$ are presented in Fig. 3. Loop parameters $\theta_{K,r}$, $\theta_{K,e}$, and H_c are given in Fig. 4 as a function of T. With increasing T, the remanence $\theta_{K,r}$ decreases rapidly when approaching $T=210$ K. We interprete this temperature as the Curie temperature of the DL stripes, which for $\Theta=1.2$ happens to coincide with the Curie temperature of the monolayer stripes.

A unique phenomenon observed in the sample of Fig. 3 and 4 and in similar samples near $\Theta=1.2$ is given by the dramatic increase of H_c with decreasing temperature, as observed in the loops of Fig. 3 and shown separately in Fig. 4(b). Within a temperature range of only 50 K (210 K$>T>$160 K), H_c increases by 3 orders of magnitude.

The magnetic behavior of the samples changes upon aging in UHV. Figure 5 shows results obtained from a wedge-shaped sample of coverage $\Theta=1.0-1.5$ at a constant temperature $T=165$ K. The wedge was scanned from $\Theta=1$ to $\Theta=1.5$ and the data were measured in three sequential series shown in Fig. 5. Both the onset of the perpendicular signal $\theta_{K,e}$ [Fig. 5(a)] and the divergence of the coercive field H_c [Fig. 5(b)] is shifted to larger coverages with increasing exposure. Besides this shift the gross behavior remains unchanged for exposures below 1 Langmuir. For exposures above 1 Langmuir, the magnetic properties are changed qualitatively, as shown in Fig. 6 and 7.

Figures 6(a) and 6(b) show longitudinal and polar loops, respectively, for progressing exposure for a sample with $\Theta=1.4$ measured at $T=165$ K. Corresponding loop parameters are given in Figs. 7(a)–7(c). The data reveal an increase

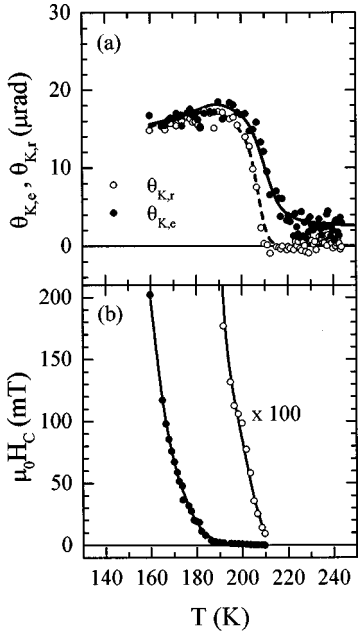

FIG. 4. (a) Extrapolated and remanent Kerr rotation $\theta_{K,e}$ (full circles) and $\theta_{K,r}$ (open circles), taken from Kerr loops for $\Theta = 1.2$ as shown in Fig. 3, versus temperature. (b) Coercive force H_c, taken from Kerr loops as shown in Fig. 3, versus temperature.

of the longitudinal extrapolation $\epsilon_{K,e}$ [Fig. 7(a)] and a decrease of the polar one $\theta_{K,e}$ [Fig. 7(b)]. A discussion of this behavior will be given below.

The data suggest a rotation of the DL magnetization during residual gas adsorption at exposures between 0.5 and 2 Langmuirs. A rotation of the easy axis from the normal [110] to the in-plane axis $[1\bar{1}0]$ is suggested by the increase of the longitudinal extrapolation $\epsilon_{K,e}$ in Fig. 7(a) and the decrease

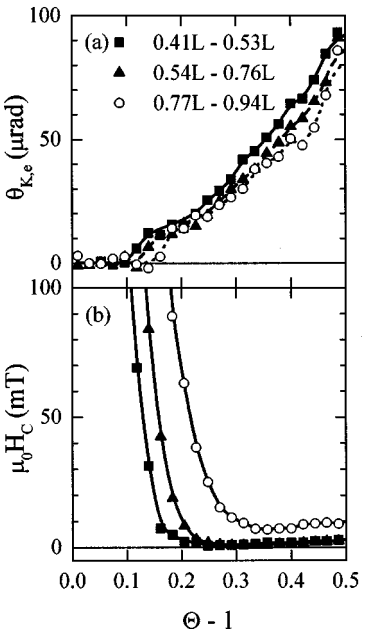

FIG. 5. (a) Extrapolated Kerr rotation $\theta_{K,e}$ and (b) coercive force H_c as a function of double layer coverage $\Theta - 1$ with exposure to residual gas given in Langmuirs as a parameter ($1L = 10^{-6}$ Torr sec).

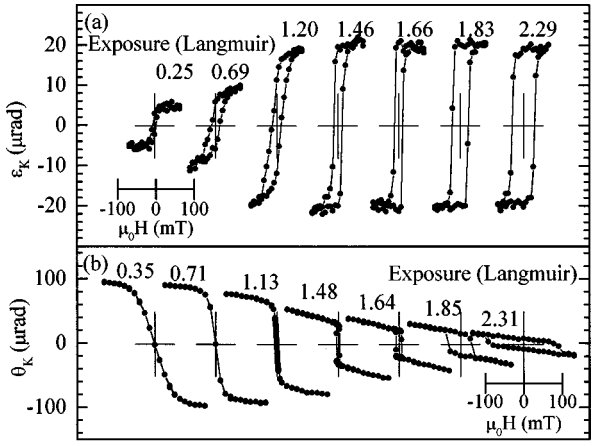

FIG. 6. Longitudinal (a) and polar (b) Kerr loops measured at $T = 165$ K for a sample of coverage $\Theta = 1.4$ with increasing exposure to residual gases. The sample was prepared at $Q > 15$ AL/L (see the text for the definition of the quality factor Q).

of the polar one $\theta_{K,e}$ in Fig. 7(b). However, an alternative interpretation without rotation of the easy axis assumes a decrease of the perpendicular anisotropy. A most prominent

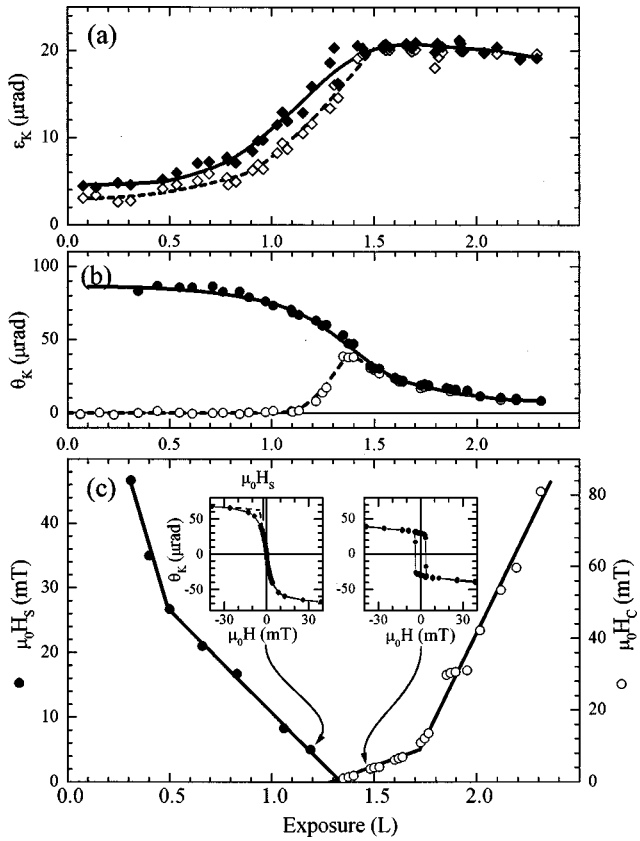

FIG. 7. Parameters of loops like those in Fig. 6 versus residual gas exposure. (a) Extrapolated value of the longitudinal Kerr ellipticity $\epsilon_{K,e}$ (closed diamonds) and remanence $\epsilon_{K,r}$ (open diamonds), respectively. (b) Extrapolated value of the polar Kerr rotation $\theta_{K,e}$ (closed circles) and remanence $\theta_{K,r}$ (open circles), respectively. (c) Saturation field $\mu_0 H_s$ from reversible loops for exposures below 1.3 L (closed circles) and coercive field $\mu_0 H_c$ from easy axis loops observed for exposures above 1.3 L (open circles). Typical loops as insets.

feature of the polar loops is the sudden change from reversible loops for exposures below 1.2 L to easy-axis-like square loops above 1.4 L. This change can be seen directly in the loops of Fig. 6(b). It shows up in Fig. 7(b) by the sharp rise of $\theta_{K,r}$ from zero to $\theta_{K,e}$, and in Fig. 7(c) by the decrease of the saturation field H_s (as defined in the inset) below 1.3 L and in the increase of H_c above 1.3 L.

V. DISCUSSION

The onset of perpendicular remanence observed in the polar Kerr loops proceeds with increasing coverage $\Theta > 1.1$ AL (Fig. 2) or increasing adsorption of residual gases above 1.3 L [Fig. 7(b)]. Because of the qualitatively different explanation for these two experimental phenomena the discussion is devided in two parts.

A. Onset of perpendicular remanence with increasing coverage

The onset of perpendicular remanence with increasing coverage is accompanied by the following unusual experimental phenomena different from common ultrathin film behavior.

(i) The onset of a perpendicular signal occurs for coverages $\Theta > 1.1$ only, whereas it is expected at $\Theta = 1$ for the case of independent perpendicularly magnetized stripes [see Fig. 2(a)].

(ii) Near the onset of the perpendicular remanence the polar Kerr loops show a hysteretic inner section for small fields and a reversible linear increase for larger fields (see Fig. 3 at $T = 188$ K). Similar Kerr loops would be expected for homogeneous films with a canted uniaxial anisotropy.

(iii) The coercive field H_c diverges both with decreasing Θ upon approaching the critical coverage $\Theta = 1.1$ (see Fig. 2) and with decreasing temperature below 200 K [see Fig. 4(b)]. Within a temperature range of only 50 K, H_c shows a dramatic increase by 3 orders of magnitude.

These unusual phenomena can be explained using a micromagnetic model[22] consisting of a periodic array of stripes with alternating orthogonal uniaxial anisotropies. Despite the discontinuous change of anisotropy from a perpendicular easy axis in the DL stripe to an in-plane easy axis in the ML-stripe, the magnetization direction will change continuously on a lateral scale given by the exchange length. The magnetization direction is specified by the angle $\vartheta(x)$ with respect to the film normal as a function of the x coordinate along the $[1\bar{1}0]$ direction (across the stripe array). With a_{DL} and a_{ML} being the width of the DL stripe and the ML stripe, respectively, and $x = 0$ denoting the boundary between the DL region for $x < 0$ and the ML region for $x > 0$, $\vartheta(x)$ results from the minimization of the free energy γ per period $L = a_{\mathrm{DL}} + a_{\mathrm{ML}} = 9$ nm:

$$\gamma = 2 \int_{-a_{\mathrm{DL}}/2}^{+a_{\mathrm{ML}}/2} \left\{ A_i t_i \left(\frac{d\vartheta}{dx} \right)^2 + K_i t_i \sin^2 \vartheta \right\} dx. \qquad (5.1)$$

Exchange stiffness A_i, anisotropy constant K_i and film thickness t_i are constants except for a discontinuous change at $x = 0$ ($i = \mathrm{DL}$ for $x < 0$ and $i = \mathrm{ML}$ for $x > 0$). The variational problem given by Eq. (5.1), was solved analytically.[22]

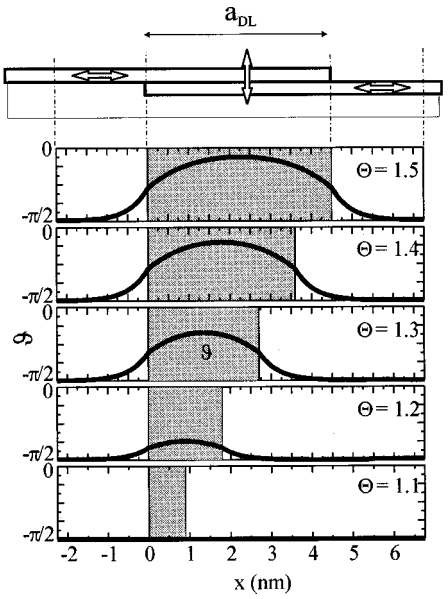

FIG. 8. Numerical results from micromagnetic theory for the magnetization direction $\vartheta(x)$ as a function of the x coordinate across a periodic stripe array of width $L = a_{\mathrm{ML}} + a_{\mathrm{DL}} = 9$ nm. The width of the double layer stripe a_{DL} is varied, corresponding to a coverage of $\Theta = 1 + a_{\mathrm{DL}}/L$. Parameters used for the calculation: $K_{\mathrm{ML}} = -5 \times 10^6$ Jm^{-3}, $K_{\mathrm{DL}} = +1 \times 10^6$ Jm^{-3}, $A = \times 10^{-12}$ J/m.

One main result is the observation that $\vartheta(x)$ will switch into a uniform in-plane state [$\vartheta(x) = \pi/2$] if the DL stripe width is reduced below a critical value $a_{\mathrm{DL},c}$, which is given by

$$a_{\mathrm{DL},c} = 2 L_{\mathrm{DL}} \arctan\{\alpha \tanh(a_{\mathrm{ML}}/2L_{\mathrm{ML}})\}. \qquad (5.2)$$

$L_i = \sqrt{A_i/|K_i|}$ denotes the exchange lengths and $\alpha = \sqrt{(A_{\mathrm{ML}}|K_{\mathrm{ML}}|t_{\mathrm{ML}}^2)/(A_{\mathrm{DL}}|K_{\mathrm{DL}}|t_{\mathrm{DL}}^2)}$ is a parameter of the order of 1.

The existence of a critical width $a_{\mathrm{DL},c} > 0$ qualitatively explains the phenomena (i) of delayed perpendicular magnetization. For a quantitative discussion we take effective values for the anisotropy constants K_i determined from torsion oscillation magnetometry, $K_{\mathrm{ML}} = -5 \times 10^6$ Jm^{-3} for the monolayer[12] and $K_{\mathrm{DL}} = +1 \times 10^6$ Jm^{-3} for double layer islands.[17] For simplicity we assume $A_{\mathrm{ML}} = A_{\mathrm{DL}} = A$, finding $\alpha = 1.118$. $a_{\mathrm{DL},c}$ depends on the width a_{ML} of the monolayer stripe. However, if as in our case $\tanh(a_{\mathrm{ML}}/2L_{\mathrm{ML}}) \approx 1$, Eq. (5.2) will take the approximate form $a_{\mathrm{DL},c} \approx 1.7 L_{\mathrm{DL}}$. In our experiment the onset of perpendicular magnetism is delayed up to a coverage $\Theta = 1.1$ corresponding to a DL stripe width $a_{\mathrm{DL}} = 0.9$ nm. Thus the exchange length within the DL area is roughly $L_{\mathrm{DL}} \approx 0.5$ nm, and this corresponds to an exchange constant $A \approx \times 10^{-12}$ J/m, which is an order of magnitude smaller than the value for bulk Fe. A smaller value for A in ultrathin Fe/W(110) films seems reasonable taking into account the following argument: Within the mean field model A could be derived from $T_c \propto zA$ with the number of nearest neighbors z. The Curie-temperature of the monolayer $T_c(\mathrm{ML}) = 225$ K is considerably below $0.5 T_{c,\mathrm{bulk}}$, which could be expected from the ratio of nearest neighbors in the monolayer compared to the bulk value, and thus suggests a lower value for A.[24]

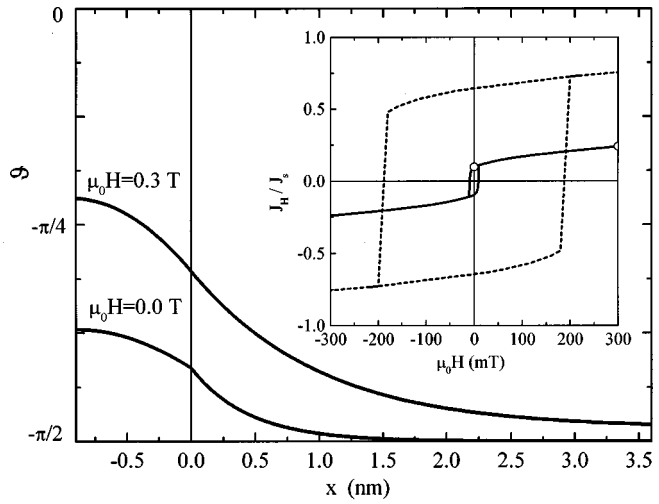

FIG. 9. Numerical results for $\vartheta(x)$ from micromagnetic theory as in Fig. 8 with external field H as parameter. The width of the double layer stripe was chosen $a_{\mathrm{DL}}=1.8$ nm, corresponding to a coverage of $\Theta=1.2$. The inset shows perpendicular magnetization loops resulting from integration of $\vartheta(x)$ for double layer widths corresponding to $\Theta=1.2$ (full line) and $\Theta=1.4$ (broken line).

Numerical calculations for the magnetization direction $\vartheta(x)$ are shown in Fig. 8, to quantitatively illustrate the sudden onset of a perpendicular remanent magnetization near a coverage $\Theta=1.1$, i.e., at a critical width $a_{\mathrm{DL},c}=0.9$ nm. Note that $\vartheta(x)$ shows a kink at $x=0$ resulting from the condition that $A_i^* t_i \vartheta'(x)$ be continuous. This condition means that the torque on the magnetization be continuous at $x=0$, analogously to the mechanic torque within a wire which discontinuously changes its diameter.

In order to calculate magnetization curves we include an appropriate Zeeman term in Eq. (5.1). As shown in Fig. 9, an external field along the film normal preferably acts on the magnetization direction in the double layer area which in the remanent state is oriented approximately along $\vartheta=45°$. The nearly linear increase of the integrated magnetization with H at larger fields reproduces the experimentally observed Kerr loops at $\Theta=1.2$ [see the inset of Fig. 2(a) and Fig. 3].

The diverging of H_c (iii) can be understood, taking into account the inhomogeneous stripe width, as shown in the STM images of Fig. 1. A single DL stripe consists of narrower and wider parts. Upon approaching the critical width, the narrow parts remain in an in-plane magnetization state, whereas the magnetization has a perpendicular component in the wider parts. During the process of magnetization reversal every wide part has to be switched separately. The wide parts thus behave similarly to a set of single domain particles where the coercive field is determined by the effective anisotropy field. If the mean width becomes wider for increasing coverage, perpendicular magnetization components will develop along the whole stripe. Consequently, the magnetization reversal takes place by domain wall movement known to result in reduced coercive fields.

A similar consideration explains the divergence of H_c with decreasing temperature observed for coverages just above the critical coverage (Fig. 4). Monolayer stripes become ferromagnetic below Curie temperatures $T_c \approx 200$ K.[11] Above this temperature the paramagnetic ML stripes provide only a vanishing exchange force, leaving the blocking of domain walls in narrow parts of the DL stripes ineffective. Below this temperature the exchange energy creates in-plane magnetized parts in these narrow parts, thus blocking the domain wall movement as described above. The dramatic increase of H_c by 3 orders of magnitude takes place in the narrow temperature range 160 K$<T<$210 K because the monolayer stripes become ferromagnetic in a narrow temperature range, determined by the distribution of stripe widths and the dependence of the Curie temperature on the stripe width.[11]

B. Onset of perpendicular remanence with increasing residual gas adsorption

A prominent experimental result, shown in Figs. 6 and 7, is given by the sudden onset of perpendicular remanence $\theta_{K,r}$ with increasing adsorption of residual gas. Previously seen as an experimental obstacle we will now exploit this feature for a deeper understanding of the interplay of exchange coupling, dipolar coupling and perpendicular anisotropy. In DL islands,[19] the residual gas adsorption reduces the perpendicular anisotropy, the same can be expected for DL stripes. A reduction of perpendicular anisotropy results in an increase of the exchange length and hence in an increase of the critical width for the onset of perpendicular magnetization [see Eq. (5.2)], which can be observed in the experiment too (Fig. 5). This agreement further confirms the assumption of a reduced perpendicular anisotropy. We shall discuss the onset of perpendicular remanence along the following guideline: For clean samples, the dipolar antiferromagnetic coupling suppresses perpendicular remanence $\theta_{K,r}$ for $\Theta>1.25$.[21] The dipolar antiferromagnetic coupling decreases with decreasing perpendicular anisotropy, finally resulting in a perpendicular remanence.

The idea of dipolar antiferromagnetic coupling is supported by the following consideration. The perpendicular signal saturates in quite low fields. Defining a saturation field H_s by the intercept of the initial linear section and the final saturation section, we obtained values of $\mu_0 H_s \approx 20$ mT. These low values suggest that the demagnetized remanent state can be explained by an antiferromagnetic dipolar coupling between the perpendicularly magnetized DL stripes resulting in an antiferromagnetic array of up and down magnetized stripes. In finite external fields the system apparently adjusts by reversible movement of domain walls between alternatingly magnetized sections of single stripes, resulting in the initial linear increase of the perpendicular signal.

For a quantitative estimate of H_s, we compare H_s with the dipolar stray field $\vec{H}_d$ which one stripe in a homogeneously magnetized system of DL stripes would feel by the interaction with all other stripes. $\vec{H}_d$ can be deduced from magnetostatic theory in the limit of narrow, homogeneously magnetized and parallel DL stripes, neglecting the magnetic moments of the monolayer stripes. Denoting $W_0 a_{\mathrm{W}}$ the distance of atomic rows between adjecent DL stripes, a_{W} the lattice constant and $\vec{\mu}=\mu[\sin\vartheta;0;\cos\vartheta]$ the atomic moment which is canted in the x-z plane by a polar angle ϑ with respect to the film normal, one obtains for a DL coverage $\Theta_{\mathrm{DL}}=\Theta-1$:

$$\vec{H}_d = (2\pi/3)(\mu\Theta_{\mathrm{DL}}/W_0 a_{\mathrm{W}}^3)[\sin\vartheta; 0; -\cos\vartheta]. \quad (5.3)$$

Equation (5.3) is a good approximation for $\Theta_{\mathrm{DL}} < 0.6$. Assuming $\vartheta = 0$, we obtain an antiferromagnetic coupling field $\mu_0 H_d = 21$ mT for $\Theta_{\mathrm{DL}} = 0.5$ and $\mu = 2.2\ \mu_B$ which is of the same order of magnitude as the experimentally observed values at $T = 165$ K [see, for example, the inset of Fig. 2(b) and Fig. 7 for for exposures below 0.5 L]. This agreement strongly supports the simple model of dipolar coupling in this temperature range. However, for some samples prepared under extremely clean conditions we observed increasing values up to $\mu_0 H_s = 120$ mT with decreasing temperature below $T < 150$ K, which does not agree with the dipolar coupling model and remains to be explained.

The decrease of perpendicular anisotropy during residual gas adsorption not only shifts the critical width [see Eq. (5.2) and Fig. 5] but will also increase the canting angle ϑ_0 in the center of the DL stripe because of the increase of exchange length (see Fig. 8). In the following we assign $\vartheta = \vartheta_0$ for simplicity. Two distinct models for the change of the perpendicular anisotropy are discussed. In the first model (A) we assume a perpendicular uniaxial anisotropy in the DL stripes decreasing in strength with increasing residual gas adsorption. In this case the two canting angles ϑ and $-\vartheta$ are equivalent. In a second model (B) we consider an energetic asymmetry of the two angles ϑ and $-\vartheta$. This asymmetry might be the result of the geometrical step-down–step-up asymmetry of the vicinal substrate.

In model (A), the perpendicular components of the magnetization in the DL stripes order antiferromagnetically whereas the in-plane components are parallel. In this case only the perpendicular component of the demagnetizing field given in Eq. (5.3) contributes to the antiferromagnetic coupling field. Hence, the decreasing value of H_s for increasing exposure as shown in Fig. 7(c) directly results from the decrease of the perpendicular component of $\vec{H}_d$ with increasing angle ϑ [see Eq. (5.3)]. However, one would expect H_s to disappear at the same time as ϑ approaches 90°, in contrast to the experimental observation. From the extrapolated Kerr signals shown in Figs. 7(a) and 7(b), one estimates $\vartheta = 50°$ for an exposure of 1.3 L, which can be taken from Fig. 7(c) as characteristic for $H_s = 0$. For an explanation of this discrepancy one might assume an additional effective coupling given by the exchange energy favoring a parallel alignment of the perpendicular magnetization components. As can be concluded from Fig. 8 this contribution is rather small because the magnetization direction in the center of the ML stripe is very close to the in-plane direction thus providing no preference for the direction of magnetization in the adjacent DL stripe. A second possibility could be a metastable ferromagnetic state stabilized by the blocking of domain wall movement, i.e., the coercive field. However, it is difficult to explain the sudden change from reversible loops for exposures below 1.2 L, to easy-axis-like square loops above 1.4 L [see Fig. 7(c)], considering the broad distribution of stripe widths and hence of H_c.

In model (B), we assume that the energetic minima of the two axes defined by ϑ and $-\vartheta$ differ substantially, forcing the magnetization in the DL stripes to orient along only one of the two axes. The perpendicular components of the magnetization in the DL stripes again order antiferromagnetically whereas now the in-plane components are antiparallel, too. Equation (5.3) then shows that for $\vartheta = 45°$ the coupling switches from antiferromagnetic to ferromagnetic, because $\vec{\mu}$ is at right angles to $\vec{H}_d$. This explains the sudden change from antiferromagnetic to ferromagnetic alignment of the DL magnetization in Fig. 7 at 1.3 L. The critical angle $\vartheta = 50°$ determined from experiment [Figs. 7(a) and 7(b) is very close the predicted value, thus supporting model (B). However, the remanent in-plane magnetization observed in Fig. 7(a) emerging considerably before an exposure of 1.3 L is reached, is in contradiction to this model. In both models, the linear increase of the polar Kerr signal with external field can be interpreted as a rotation of the canted magnetization angle ϑ within the DL stripe.

VI. CONCLUSIONS

In conclusion, we observed the onset of prependicular magnetization in Fe(110) nanostripe arrays on W(110) for coverages between 1 and 2 atomic layers. The one-dimensional geometry of the samples eases the application of a micromagnetic model. The magnetic easy axis in the as-prepared samples switches from in-plane in the monolayer to perpendicular in the double layer stripes. Beyond a critical width a remanent perpendicular order occurs in the double layer stripes. Micromagnetic calculations show that this is a result of the exchange interaction. They explain the dramatic increase of the coercive force by 3 orders of magnitude with decreasing temperature. Magnetostatic interactions induce antiferromagnetic interstripe coupling resulting in reversible magnetization loops for sesquilayers. During residual gas exposure, the magnetization direction rotates into the plane, resulting in a sharp transition from antiferromagnetic to ferromagnetic interstripe coupling. Different models for this transition remain to be checked.

The insight into the various coupling phenomena gained from the simple one-dimensional geometry of the nanostripe array greatly helps to understand the seemingly contradictory results of Fe sesquilayers deposited at room temperature on smooth W(110).[12–15,17] The experimental parameter window for the preparation of sesquilayers with perpendicular remanence is exceptionally small. If the DL islands are too small the exchange energy causes the magnetization to stay completely in the film plane. For larger islands the increasing antiferromagnetic dipolar coupling between DL islands results in a compensation of the perpendicular magnetization components. Coercive fields in this state may be huge because the DL islands behave as single domain particles and thus effectively prevent a detection of a perpendicular signal by Kerr magnetometry. Finally the perpendicular anisotropy of the DL apparently is a result of the 10% pseudomorphic strain and therefore must be expected to disappear if the island or stripe width along $[1\bar{1}0]$ exceeds 9 nm and consequently misfit dislocations are created for relaxation of this pseudomorphic strain.

ACKNOWLEDGMENTS

This work was supported by the Deutsche Forschungsgemeinschaft.

[1] P. Grünberg, R. Schreiber, Y. Pang, M. B. Brodsky, and H. Sowers, Phys. Rev. Lett. **57**, 2442 (1986).
[2] S. S. P. Parkin, N. More, and K. P. Roche, Phys. Rev. Lett. **64**, 2304 (1990).
[3] J. Unguris, R. J. Celotta, and D. T. Pierce, Phys. Rev. Lett. **67**, 140 (1991).
[4] M. N. Baibich, J. M. Broto, A. Fert, F. Nguyen van Dau, F. Petroff, P. Etienne, G. Creuzet, A. Friederich, and J. Chazelas, Phys. Rev. Lett. **61**, 2472 (1988).
[5] G. Binasch, P. Grünberg, F. Saurenbach, and W. Zinn, Phys. Rev. B **39**, 4828 (1989).
[6] S. Y. Chou, P. R. Krauss, and L. Kong, J. Appl. Phys. **79**, 6101 (1996).
[7] M. A. M. Gijs, A. Reinders, R. M. Jungblut, W. Oepts, and W. J. M. de Jonge, J. Magn. Magn. Mater. **165**, 17 (1997).
[8] A. Sugawara, T. Coyle, G. G. Hembree, and M. R. Scheinfein, Appl. Phys. Lett. **70**, 1043 (1997).
[9] T. Jung, R. Schlittler, J. K. Gimzewski, and F. J. Himpsel, Appl. Phys. A: Mater. Sci. Process. **61**, 467 (1995).
[10] J. Shen, R. Skomski, M. Klaua, H. Jenniches, S. Sundar Manoharan, and J. Kirschner, Phys. Rev. B **56**, 2340 (1997).
[11] J. Hauschild, H. J. Elmers, and U. Gradmann, Phys. Rev. B **57**, R677 (1998).
[12] H. J. Elmers, J. Hauschild, H. Fritzsche, G. Liu, U. Gradmann, and U. Köhler, Phys. Rev. Lett. **75**, 2031 (1995).
[13] D. Sander, R. Skomski, C. Schmidthals, A. Enders, and J. Kirschner, Phys. Rev. Lett. **77**, 2566 (1996).
[14] J. H. Suen and J. H. Erskine, Phys. Rev. Lett. **78**, 3567 (1997).
[15] D. Sander, A. Enders, R. Skomski, and J. Kirschner, IEEE Trans. Magn. **32**, 4570 (1996).
[16] M. Kolesik, M. A. Novotny, and Per Arne Rikvold, Phys. Rev. B **56**, 11 791 (1997).
[17] N. Weber, K. Wagner, H. J. Elmers, J. Hauschild, and U. Gradmann, Phys. Rev. B **55**, 14 121 (1997).
[18] H. J. Elmers, N. Weber, K. Wagner, J. Hauschild, and U. Gradmann, in *Magnetic Ultrathin Films, Multilayers and Surfaces—1997*, edited by D. D. Chambliss *et al.*, MRS Symposia Proceedings No. 475 (Materials Research Society, Pittsburgh, 1998), p. 189.
[19] T. Dürkop, H. J. Elmers, and U. Gradmann, J. Magn. Magn. Mater. **172**, L1 (1997).
[20] M. Bode, R. Pascal, and R. Wiesendanger, J. Vac. Sci. Technol. A **15**, 1285 (1997).
[21] J. Hauschild, H. J. Elmers, and U. Gradmann, Appl. Phys. Lett. **72**, 3211 (1998).
[22] H. J. Elmers, J. Magn. Magn. Mater. **185**, 274 (1998).
[23] H. Hornauer, T. M. Atmono, and K. Rll, J. Magn. Magn. Mater. **83**, 551 (1990).
[24] A. Gangulee and R. J. Kobliska, J. Appl. Phys. **49**, 4896 (1978).
[25] C. Jensen, K. Reshöft, and U. Köhler, Appl. Phys. A: Mater. Sci. Process. **62**, 217 (1996).